Research Article | Vol. 25, No. 15 | 24 Jul 2017 | OPTICS EXPRESS 17105
Optics EXPRESS

Label-free detection of bovine serum albumin based on an in-fiber Mach-Zehnder interferometric biosensor

ZHENGYONG LI,[1] CHANGRUI LIAO,[1,4] DANNI CHEN,[1] JUN SONG,[1] WEI JIN,[2] GANG-DING PENG,[3] FENG ZHU,[1] YING WANG,[1] JUN HE,[1] AND YIPING WANG[1,5]

[1]*Key Laboratory of Optoelectronic Devices and Systems of Ministry of Education and Guangdong Province, College of Optoelectronic Engineering, Shenzhen University, Shenzhen 518060, China*
[2]*Department of Electrical Engineering, The Hong Kong Polytechnic University, Hong Kong, China*
[3]*School of Electrical Engineering and Telecommunications, University of New South Wales, Sydney 2052, NSW, Australia*
[4]*cliao@szu.edu.cn*
[5]*ypwang@szu.edu.cn*

Abstract: We propose and experimentally verify an innovative label-free optical fiber biosensor based on a Mach-Zehnder interferometer for bovine serum albumin (BSA) concentration detection. The proposed fiber biosensor utilized a micro-cavity within a single-mode fiber to induce Mach-Zehnder interference. A remarkable feature of this biosensor is that external media can directly interact with the fiber core signal through microfluidic channels connected to the micro-cavity and sensor surface. The device was fabricated by means of femtosecond laser micromachining and chemical etching. A fiber interferometer of this type exhibits an ultrahigh refractive index sensitivity of −10,055 nm/RIU and a detection limit of 3.5×10^{-5} RIU. Different concentrations of BSA with an infinitesimally small refractive index difference can be clearly differentiated in situ by the interferential spectra of the structure. Experiments demonstrated the biosensor exhibited a BSA solution concentration sensitivity of −38.9 nm/(mg/mL) and a detection limit of 2.57×10^{-4} mg/mL, respectively. Moreover, this biosensor is a sub-microliter dose and ultrasensitive at the low concentrations detected in BSA, which make it a promising for biochemical applications such as DNA hybridization, cancer screenings, medicine examination and environmental engineering, etc.

OCIS codes: (060.2300) Fiber measurements; (060.2370) Fiber optics sensors; (170.1420) Biology; (230.4000) Microstructure fabrication.

References and links

1. C. Liao, S. Liu, L. Xu, C. Wang, Y. Wang, Z. Li, Q. Wang, and D. N. Wang, "Sub-micron silica diaphragm-based fiber-tip Fabry-Perot interferometer for pressure measurement," Opt. Lett. **39**(10), 2827–2830 (2014).
2. T. Guo, B. O. Guan, and J. Albert, "Tilted fiber grating mechanical and biochemical sensors," Opt. Laser Technol. **78**, 19–33 (2016).
3. S. Sridevi, K. S. Vasu, S. Asokan, and A. K. Sood, "Sensitive detection of C-reactive protein using optical fiber Bragg gratings," Biosens. Bioelectron. **65**, 251–256 (2015).
4. W. C. Wang, C. C. Chan, J. L. Boo, Z. Y. Teo, Z. Q. Tou, H. B. Yang, C. M. Li, and K. C. Leong, "Photonic Crystal Fiber Surface Plasmon Resonance Biosensor Based on Protein G Immobilization," IEEE J. Quantum Electron. **19**(3), 4206107 (2013).
5. A. Urrutia, K. Bojan, L. Marques, K. Mullaney, J. Goicoechea, S. James, M. Clark, R. Tatam, and S. Korposh, "Novel Highly Sensitive Protein Sensors Based on Tapered Optical Fibres Modified with Au-Based Nanocoatings," J. Sens. **2016**, 1–11 (2016).
6. R. G. Heideman, R. P. H. Kooyman, and J. Greve, "Performance of a highly sensitive optical waveguide Mach-Zehnder interferometer immunosensor," Actuator B-Chem. **10**(3), 209–217 (1993).
7. F. Brosinger, H. Freimuth, M. Lacher, W. Ehrfeld, E. Gedig, A. Katerkamp, F. Spener, and K. Cammann, "A label-free affinity sensor with compensation of unspecific protein interaction by a highly sensitive integrated optical Mach-Zehnder interferometer on silicon," Sens. Actuator B-Chem. **44**(1–3), 350–355 (1997).

#296259 https://doi.org/10.1364/OE.25.017105
Journal © 2017 Received 17 May 2017; revised 16 Jun 2017; accepted 19 Jun 2017; published 10 Jul 2017

Optics EXPRESS

8. B. J. Luff, J. S. Wilkinson, J. Piehler, U. Hollenbach, J. Ingenhoff, and N. Fabricius, "Integrated Optical Mach-Zehnder Biosensor," J. Lightwave Technol. **16**(4), 583–592 (1998).
9. Q. Liu, X. Tu, K. W. Kim, J. S. Kee, Y. Shin, K. Han, Y. J. Yoon, G. Q. Lo, and M. K. Park, "Highly sensitive Mach–Zehnder interferometer biosensor based on silicon nitride slot waveguide," Actuator B-Chem. **188**, 681–688 (2013).
10. F. Preieto, B. Sepulveda, A. Calle, A. Llobera, C. Dominguez, and L. M. Lechuga, "Integrated Mach-Zehnder interferometer based on ARROW structures for biosensor applications," Sens. Actuator B-Chem. **92**(1–2), 151–158 (2003).
11. S. H. Hsu and Y. T. Huang, "A novel Mach-Zehnder interferometer based on dual-ARROW structures for sensing applications," J. Lightwave Technol. **23**(12), 4200–4206 (2005).
12. B. Sun, Y. Huang, S. Liu, C. Wang, J. He, C. Liao, G. Yin, J. Zhao, Y. Liu, J. Tang, J. Zhou, and Y. Wang, "Asymmetrical in-fiber Mach-Zehnder interferometer for curvature measurement," Opt. Express **23**(11), 14596–14602 (2015).
13. J. H. Lim, H. S. Jang, K. S. Lee, J. C. Kim, and B. H. Lee, "Mach-Zehnder interferometer formed in a photonic crystal fiber based on a pair of long-period fiber gratings," Opt. Lett. **29**(4), 346–348 (2004).
14. L. V. Nguyen, D. Hwang, S. Moon, D. S. Moon, and Y. Chung, "High temperature fiber sensor with high sensitivity based on core diameter mismatch," Opt. Express **16**(15), 11369–11375 (2008).
15. H. Y. Choi, K. S. Park, and B. H. Lee, "Photonic crystal fiber interferometer composed of a long period fiber grating and one point collapsing of air holes," Opt. Lett. **33**(8), 812–814 (2008).
16. J. J. Zhu, A. P. Zhang, T. H. Xia, S. L. He, and W. Xue, "Fiber-Optic High-Temperature Sensor Based on Thin-Core Fiber Modal Interferometer," IEEE Sens. J. **10**(9), 1415–1418 (2010).
17. Z. Li, C. Liao, Y. Wang, X. Dong, S. Liu, K. Yang, Q. Wang, and J. Zhou, "Ultrasensitive refractive index sensor based on a Mach-Zehnder interferometer created in twin-core fiber," Opt. Lett. **39**(17), 4982–4985 (2014).
18. Z. B. Tian, S. S. H. Yam, J. Barnes, W. Bock, P. Greig, J. M. Fraser, H. P. Loock, and R. D. Oleschuk, "Refractive index sensing with Mach-Zehnder interferometer based on concatenating two single-mode fiber tapers," IEEE Photonics Technol. Lett. **20**(8), 626–628 (2008).
19. J. Yang, L. Jiang, S. Wang, B. Li, M. Wang, H. Xiao, Y. Lu, and H. Tsai, "High sensitivity of taper-based Mach-Zehnder interferometer embedded in a thinned optical fiber for refractive index sensing," Appl. Opt. **50**(28), 5503–5507 (2011).
20. Y. F. Geng, X. J. Li, X. L. Tan, Y. L. Deng, and X. M. Hong, "Compact and Ultrasensitive Temperature Sensor With a Fully Liquid-Filled Photonic Crystal Fiber Mach-Zehnder Interferometer," IEEE Sens. J. **14**(1), 167–170 (2014).
21. Z. Li, C. Liao, Y. Wang, L. Xu, D. Wang, X. Dong, S. Liu, Q. Wang, K. Yang, and J. Zhou, "Highly-sensitive gas pressure sensor using twin-core fiber based in-line Mach-Zehnder interferometer," Opt. Express **23**(5), 6673–6678 (2015).
22. J. T. Zhou, Y. P. Wang, C. R. Liao, G. L. Yin, K. M. Yang, X. Y. Zhong, Q. Wang, and Z. Y. Li, "Intensity-Modulated Strain Sensor Based on Fiber In-Line Mach-Zehnder Interferometer," IEEE Photonics Technol. Lett. **26**(5), 508–511 (2014).
23. S. S. Zhang, W. G. Zhang, P. C. Geng, and L. Wang, "A Mach-Zehnder interferometer constructed using lateral offset and a long period fiber grating for two-dimensional bending vector sensing," J. Opt. **16**(1), 015501 (2014).
24. J. Lou, L. Tong, and Z. Ye, "Modeling of silica nanowires for optical sensing," Opt. Express **13**(6), 2135–2140 (2005).
25. B. Song, H. Zhang, B. Liu, W. Lin, and J. Wu, "Label-free in-situ real-time DNA hybridization kinetics detection employing microfiber-assisted Mach-Zehnder interferometer," Biosens. Bioelectron. **81**, 151–158 (2016).
26. Y. Wang, M. Yang, D. N. Wang, S. Liu, and P. Lu, "Fiber in-line Mach-Zehnder interferometer fabricated by femtosecond laser micromachining for refractive index measurement with high sensitivity," J. Opt. Soc. Am. B **27**(3), 370–374 (2010).
27. A. Marcinkevičius, S. Juodkazis, M. Watanabe, M. Miwa, S. Matsuo, H. Misawa, and J. Nishii, "Femtosecond laser-assisted three-dimensional microfabrication in silica," Opt. Lett. **26**(5), 277–279 (2001).
28. Y. Wang, M. Yang, D. N. Wang, S. Liu, and P. Lu, "Fiber in-line Mach-Zehnder interferometer fabricated by femtosecond laser micromachining for refractive index measurement with high sensitivity," J. Opt. Soc. Am. B **27**(3), 370–374 (2010).
29. I. M. White and X. Fan, "On the performance quantification of resonant refractive index sensors," Opt. Express **16**(2), 1020–1028 (2008).

1. Introduction

Over the past decade, the in situ detection of proteins has been extensively investigated as the analysis of proteins is of significant importance to disease and drug research, as well as biological engineering. Fiber optic sensors are a powerful detection and analysis tool for label-free protein detection. Optical fibers are a utility material for sensor design, meaning they are economic, providing easy and efficient signal delivery [1]. As a widely-used

Optics EXPRESS

photonic device, tilted fiber Bragg gratings (TFBGs) have several advantages, including high-sensitivity wavelength response, narrow line width, reflective measurement. These properties make it an excellent biosensor. TFBG operates in an evanescent cladding mode which is sensitive to the surrounding refractive index (RI). Guo et al. [2] used TFBG-detecting urinary protein variations and a protein concentration sensitivity of 5.5 dB/(mg/mL). A detection limit (DL) of 1.5×10^{-3} mg/mL was obtained. Straight FBG functions in fundamental core mode which is insensitive to events outside the fiber cladding. As a result, they need to be processed to allow the core mode to leak out of the fiber. An etched FBG coated with an anti-C-reactive protein antibody graphene-oxide complex was used to detect C-reactive proteins with a DL of 0.01mg/L [3]. Another approach uses surface plasmon resonance (SPR) technology to observe and characterize protein behavior. SPR relies on changes in RI at the substrate surface where protein binding occurs. Wang et al. [4] proposed a new SPR biosensor based on a gold-coated photonic crystal fiber. The sensor was able to monitor binding kinetics of the IgG complexes and achieved a minimum DL at a concentration of 0.267 mg/L. Like SPR sensors, tapered fiber-based devices also respond to variations in the evanescent field, arising from alterations in the outside RI. A tapered fiber, modified with Au coatings, was used to detect proteins at the lowest concentration levels of 2.5 nM [5]. However, the above biosensors usually work based on evanescent field existing close to the fiber surface and easily spread into surrounding measured solution. Therefore a large insertion loss might be introduced to the sensor in solution sensing. For SPR sensors, film coating increases the difficulty of device fabrication and the coated film easily drops out during the measurement.

Mach-Zehnder interferometers (MZIs) have been widely used in a diverse variety of sensing applications because of their ultrahigh sensitivities and flexible configurations. Conventional MZIs have two independent interferential arms, the reference arm and the sensing arm. The incident light is split at a Y junction and propagates along the two arms. A change in the RI results in an optical phase change on the sensing arm. When the two signals recombine at an output port, interference appears spontaneously. MZIs are commonly fabricated from various types of silicon dielectric waveguides, such as SiON, Si_3N_4, and silicon oxides. The first MZI-based biosensor was developed by Heideman [6]. They created an MZI on a silicon substrate for immune-sensing applications. As waveguide technologies have improved, more MZI-based biosensor types have been demonstrated. A number of engineering enhancements in structure design and material improvement for integrated MZI sensors were incorporated in this work. In order to obtain the necessary sensitivity, Brosinger et al. [7] remolded the geometrical structure of an MZI, which utilized a SiON waveguide with a ribbed structure on a silicon substrate for IgG molecular monolayer detection. An MZI structure based on glass substrates was designed by Luff, with the addition of a three-waveguide coupler at the interferometer output [8]. This sensor has the advantage of signal referencing, establishing and maintaining a sensitive operating point, in which the detection limit for protein loading is estimated at 5 pg/mm^2. In order to enhance the sensitivity, Liu et al. [9] applied an innovative design for the sensing arm of the MZI, which consisted of a slot waveguide relative to the reference strip waveguide. This new structure allowed high light-analyte interactions which guarantee high sensitivity. Another important design improvement enabled larger waveguide core dimensions without sacrificing single-mode behavior or sensitivity. This structure, based on dual anti-resonant reflecting optical waveguides (ARROWs) [10, 11], uses a reflective cladding consisting of alternating layers of high and low refractive indices to project more light above the surface of the waveguide. As a result, sensitivity is not sacrificed with larger dimensions. In order to avoid the multi-modal and cross-polarization interference appearing at the output, the waveguide MZI structure must be single polarization and single mode. In addition, the structure and input (output) signal are mutually independent, which gives rise to a lager loss.

Fiber MZIs can overcome the discussed issues because the diversified fibers can be used to fabricate the MZI, which can directly connect a signal source to detection equipment. In

Optics EXPRESS

comparison to waveguide MZIs, fiber MZIs exhibit more compact bulk, simpler fabrication, and higher sensitivity [12]. Fiber MZIs have been investigated for several decades and various types are reported in the literature, including a pair of LPGs [13], core mismatch [14], air-hole collapsing PCF [15], small core SMF [16], micro-cavity [17], and fiber tapering [18]. These MZIs can be used to measure RI [19], temperature [20], gas pressure [21], strain [22], bend vector sensing [23], etc. Fiber MZIs are well-suited for biological sample detection because of their high sensitivity and low detection limit. When used as the sensing element in an MZI, nanofibers with a diameter of 400nm and a sensing length of 1mm can achieve a DL of 4.2×10^{-4} monolayers of analytes [24]. Song et al. [25] proposed a microfiber-assisted MZI for in situ real-time DNF hybridization kinetics detection with a DL of 0.0001 pmol/μL. In summary, fiber MZIs have significant bio-sensing potential.

In this paper, we present a simple optical fiber MZI to effectively monitor changes in BSA concentration. The MZI biosensor operates with light immediately interfacing with the BSA solution. This device was fabricated by means of femtosecond laser micromachining and chemical etching. Fiber interferometers of this type exhibit ultrahigh refractive index sensitivity of −10,055 nm/RIU and a DL of 3.5×10^{-5} RIU, which enables the biosensor to distinguish very small BSA concentration variation. High concentration sensitivity of −38.9 nm/(mg/mL) is achieved with a low DL of 2.57×10^{-4} mg/mL.

2. Operating principle of MZI

The proposed schematic structure is shown in Fig. 1. A micro-cavity is formed by removing part of the fiber core at the interface between core and cladding. Four microchannels are designed to connect the micro-cavity with surrounding medium and it makes the liquid flow in or out the micro-cavity more easily and quickly. The number of microchannels is not unique. Light reaches the micro-cavity which splits incoming light into two sections. One beam remains traveling along the fiber core while the other propagates through the micro-cavity. The two output beams, with intensities denoted by I_1 and I_2, recombine in the fiber core. The phase difference between the two output beams results in interference, which affects the output intensity of the recombined beam. This resulting intensity can be expressed as:

$$I = I_1 + I_2 + 2\sqrt{I_1 I_2}\cos\left(\frac{2\pi L\Delta n}{\lambda} + \varphi_0\right) \tag{1}$$

here, λ represents wavelength, L is the length of the micro-cavity with respect to the propagation path, $\Delta n = n_{core} - n_{cavity}$ is the difference between the effective RI values of the two interference arms (where n_{core} and n_{cavity} are the effective RI values of the core material and the medium in the microchannel), and φ_0 is the phase difference. According to Eq. (1), the output intensity assumes its minimum value under the following conditions:

$$\frac{2\pi L\Delta n}{\lambda_m} + \varphi_0 = (2\mathrm{m}+1)\pi, \tag{2}$$

where m is an integer and λ_m is the wavelength of the mth-order interference dip. When the effective RI of the medium in the micro-cavity is varied, and the dip wavelength is shifted by an amount $d\lambda$, assuming the micro-cavity length L is kept constant, the sensitivity is estimated as [26]:

$$\frac{d\lambda}{d(\Delta n)} = \frac{\lambda}{\Delta n}. \tag{3}$$

According to the Eq. (2), the free spectra range (FSR), described as the space between adjacent wave crests or wave troughs, can be written as:

Optics EXPRESS

$$FSR = \frac{\lambda^2}{\Delta n \cdot L}. \quad (4)$$

The Eq. (4) indicates that FSR can be optimized by adjusting the micro-cavity length L at a given wavelength.

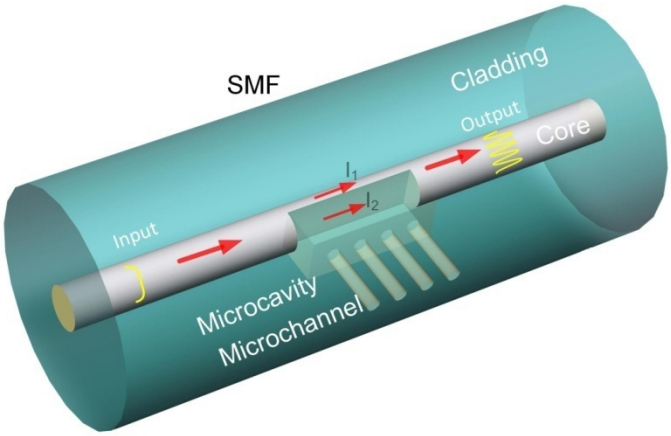

Fig. 1. A schematic diagram of the MZI-based biosensor.

3. Materials and methods

3.1 Fabrication of MZI biosensors

The sensor was fabricated on SMF (Corning, SMF-28) with the core/cladding diameters of 8/125 μm, using FS laser micromachining and chemical etching techniques. Strong focusing of FS laser can induce positive RI modification inside the fiber. Laser-modification tracks are highly susceptible to hydrofluoric acid (HF), which provides a novel means for 3D integration of optical and microfluidic components. The whole fabrication process includes two main steps: (1) inscription of the desired structure into the fiber using a tightly-focused FS beam and (2) etching of the fiber in a solution of 8% HF for selective removal of laser-modified regions.

Firstly, an MZI pattern was scribed by an FS laser. The low FS laser pulse energy modified the RI in areas exposed by the FS laser. A schematic diagram of the FS laser micromachining system is illustrated in Fig. 2(a). An FS laser (Spectra-Physics, Solstice) with a wavelength of 800 nm, a pulse duration of 120 fs, and a repetition rate of 1 kHz was used for processing. The laser beam was passed through an attenuator comprised of a half-wave plate W and a polarizer P, used to adjust the laser power in the range of 0 to 4 mJ. The light was then reflected by a beam splitter BS and focused onto the fiber by an objective lens MO with an NA value of 0.25. A shutter controlled the opening and closing of the laser and a CCD camera allowed for real-time monitoring of the micromachining process. Average on-target laser power was maintained at ~65 nJ by rotating the half-wave plate followed by the polarizer. The fiber was fixed on a computer-controlled three-axis translation stage with a resolution of 10 nm, in parallel with the Y-axis. A cuboid was scribed at the boundary between the fiber core and cladding. The treading track of the FS laser beam is shown in Fig. 2(b). The laser beam was initially focused into the center of the fiber core and then scanned along the positive X-axis at a speed of 5 μm/s across a scanning distance of 95 μm. Afterwards, the laser beam was lowered by 2 μm along the Z-axis and then scanned the same distance along the negative X-axis. The beam was then shifted along the Y-axis away from the fiber core over a distance of 1.5 μm, which constituted the first scanning cycle. The beam then scans along the positive X-axis using the same parameters, followed by a 2 μm increase

Optics EXPRESS

along the Z-axis. This is followed by a return to the left-hand end and a shift along the Y-axis, away from the fiber core over a distance of 1.5 μm. This process comprised the second scanning cycle. These two cycles were repeated until the cuboid was formed. Finally, several channels were fabricated to connect the fiber surface to the cuboid with the same parameters. High-resolution optical images of the MZI pattern are shown in Fig. 2(c). It is evident that deep-color areas were index-modified by the FS laser, whereas the RI is larger than the surrounding area.

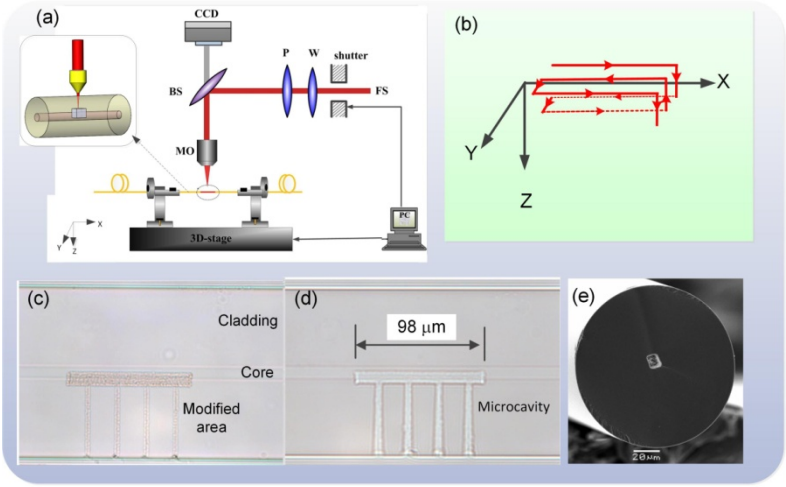

Fig. 2. (a) A schematic diagram of the FS laser micromachining system employed to fabricate the in-fiber structure. The system includes an attenuator comprised of half-wave plate (W) and polarizer (P) for adjusting the laser power, a beam splitter (BS), a CCD camera, and an objective lens (MO) for focusing the laser onto the fiber. (b) The treading track of the FS laser beam. (c) FS laser-induced index modification and (d) etching micro-cavity in the fiber. (e) The SEM image of the micro-cavity cross-section.

Secondly, the mass fraction of 40% HF solution was diluted to 8% by adding demonized water. The FS laser-inscribed fiber was immersed in an HF solution with a magnetic stirring apparatus and the ambient temperature was maintained at 40°C for ~10 min. Because microchannels connect the fiber surface, the material of modified microchannels area is firstly melted into HF solution. Then HF solution reaches the modified micro-cavity area through microchannels. Finally, material of micro-cavity is removed by HF solution. The processed fiber was visually inspected under a microscope. Images of the etched features within the fiber are shown in Fig. 2(d). Evidently, a micro-cavity and four micro-channels were achieved. The width of the channel tapers very slightly toward the micro-cavity because the inside of the fiber experiences a shorter exposure time to the HF solution, compared with regions nearer to the surface. The length of the micro-cavity was measured to be 98 μm, which is larger than the FS-inscribed area. Laser-modified features are >200 times more susceptible than an identical, unexposed fiber under the same conditions [27]. When a fiber is removed from the HF solution, further etching only serves to slightly widen the etched area. This selective etching is useful for creating various structures designed in fibers, as well as for preserving the structural integrity around the inscribed feature. A SEM image of the micro-cavity cross-section is shown in Fig. 2(e).

3.2 BSA samples preparation

BSA, also known as the fifth component, is a bovine serum globulin (shown in Fig. 3(c)) containing 583 amino acid residues with a molecular weight of 66.430 kDa. A phosphate buffer solution (PBS) of 10mM concentration, with a pH of 7.2, was used for preparation of

Optics EXPRESS

BSA samples. Prior to sample preparation, a BSA stock solution was made by dissolving 2 g of solid BSA into 100 mL of PBS. The stock solution concentration was 2 mg/mL, as shown in Fig. 3(a). In order to obtain lower concentrations, the stock solution was further diluted to prepare BSA samples. BSA concentrations ranged from 0.2 mg/mL to 2 mg/mL in increments of 0.3 mg/mL.

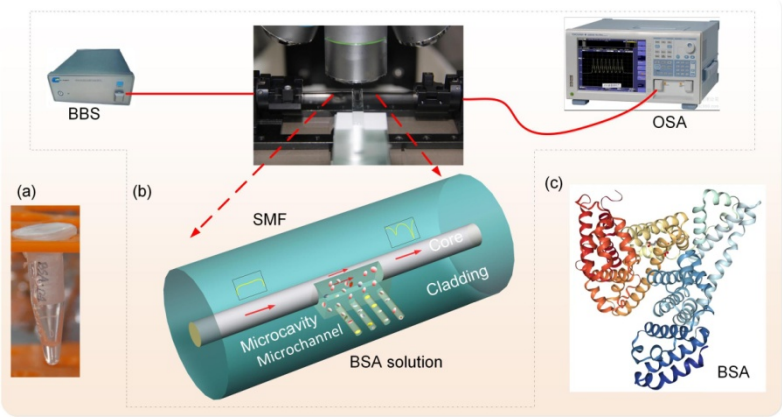

Fig. 3. The in-fiber MZI sensing system: (a) the stock BSA solution, (b) a schematic diagram of the BSA detection system, (c) a molecular BSA diagram.

3.3 Experimental setup and optical configuration

Figure 3(b) shows a schematic experimental setup of the BSA detection system. Our proposed MZI is suspended above a glass slide under a micro-objective lens. A precise pipette with rang of 1-100 μL (DragonLab) is used to move the BSA solution to the glass slide. The solution immerses over the fiber and goes into the micro-cavity based on capillarity effect. An optical microscope was used to observe BSA solution flowing into the micro-cavity in real time. Light from a broadband light source (BBS) was launched into the MZI and the interferometric transmission spectrum was monitored in real time during BSA detection procedures by employing an optical spectrum analyzer (OSA). All BSA samples were immersed over the MZI using a pipette. Sub-microliter sample volumes (~10 μL) flowed into the micro-cavity because of its small size. As such, it is well suited for the detection of micro-solution.

4. Results and discussion

4.1 RI response of the MZI biosensor

Before measuring the BSA solution, we studied the RI response of the biosensor, aiming to indirectly measure the RI of BSA solutions. The MZI-based biosensor was immersed in a series of RI liquids (Cargille Labs, http://www.cargille.com) in an RI ranging from 1.300 to 1.330 in intervals of 0.005 at room temperature. A BBS with a wavelength ranging from 1250 nm to 1650 nm and an OSA with a resolution of 0.01 nm were connected to the biosensor in order to observe transmission spectra in real time. The fiber was fixed by fiber holds which make the fiber in naturally strain status. And the experiments were carried out in clean room where temperature and humidity is stable. Hence, the influence of stress, temperature, bending and others can be avoided. Each time the sensor was removed from the tested liquid, it was carefully cleaned with alcohol to completely remove any residual liquid. When the spectrum returns to its initial state in air, a new round test can be conducted.

The original transmission spectrum of the MZI with a micro-cavity length of 98 μm in the air is shown as a black solid line in Fig. 4(a). Several interference peaks appear and the FSR is 55 nm, which was calculated to be 56 nm for λ = 1577 nm, Δn = 0.45 according to the Eq.

Optics EXPRESS

(4), where it confirms to Mach-Zehnder interference in the permitted error range. When RI liquid (n = 1.300) the micro-cavity, the FSR of the interference spectrum (shown as a red dashed line in Fig. 4(a)) is larger than the original spectrum because of a decrease in RI difference (*Δn)*. It also causes a decrease in the unguided mode loss and interface scattering loss [28], which improves insertion loss.

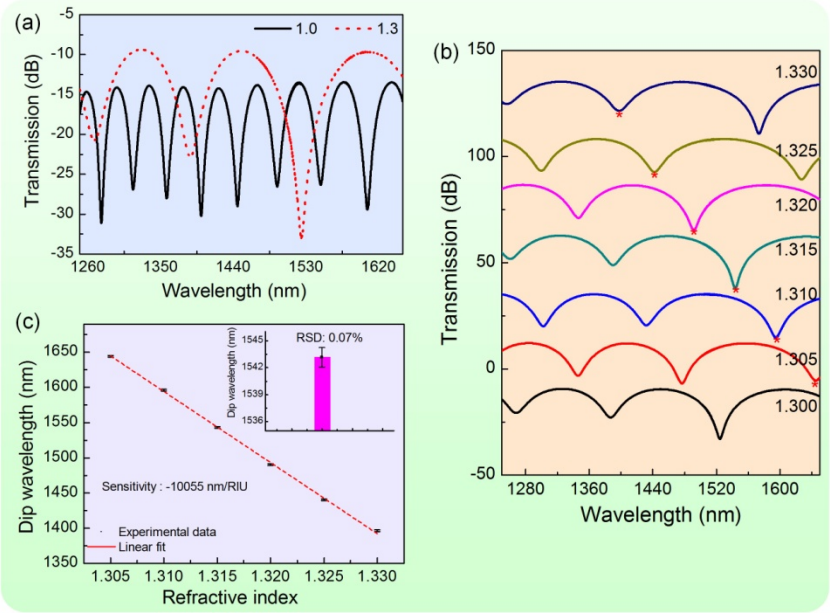

Fig. 4. (a) Interference spectra for the MZI sensor when the micro-cavity is filled with air and RI liquid (n = 1.300). (b) Transmission spectra evolution at wavelengths ranging from 1250 to 1650 nm for surrounding RI changes. (c) Dip wavelength plotted as a linear function of RI with error bars. Inset shows the average and error of the dip wavelength @1.315.

The transmission spectra of the MZI at room temperature are presented in Fig. 4(b). The fringe dip (marked by a red asterisk "*") experiences a significant blue shift when RI increases from 1.300 to 1.330. Figure 4(c) shows the dip wavelength varying with liquid RI, where a good linear wavelength response with an ultra-high sensitivity of −10,055 nm/RIU was obtained. Relative standard deviation is 0.07%. It indicates that our proposed MZI shows good repeatability that guarantees its applicability for RI sensing In contrast to other in-line fiber MZIs reported previously, the presented MZI results are caused by interference between the guided modes in the core and unguided modes travelling through the micro-cavity. The effective RI difference between the two interferometer arms was large ($\Delta n > 0.1$), which guaranteed an ultra-high RI sensitivity.

The detection limit, determined as the smallest detectable change in resonance wavelength (R) and sensitivity (S) by DL = R/S [29], is one of the norms used to evaluate the performance of various sensors. Generally, there are several factors which degrade DL, including signal-to-noise ratio (SNR), OSA resolution, thermal noise, and width of the resonance peak (FWHM). White et al. [29] theoretically and systematically investigated how these factors affect DL. In our experiment, the device was dominated by FWHM, which was measured to be ~9.7 nm. Assuming an SNR of 50 dB, the DL was calculated to be 3.5×10^{-5} RIU. This ultra-small DL allows the MZI sensor to detect tiny variations in RI. As a result, this MZI has several potential applications in chemical and biological sensing.

Optics EXPRESS

4.2 Detection of BSA samples

Experimental transmission spectra for the MZI biosensor at different BSA solution concentrations (2 mg/mL, 1.7 mg/mL, 1.4 mg/mL, 1.1 mg/mL, 0.8 mg/mL, 0.5 mg/mL, 0.2 mg/mL) are shown in Fig. 5(a). It is evident the dip wavelength (denoted by a red asterisk "*") is shifted to shorter wavelengths at a distance of 68 nm corresponding to BSA concentration. This implies increasing BSA concentrations, even through slight RI changes between them. Quantitative data are presented in Fig. 5(b), which exhibit an excellent linear fit. The ultra-high wavelength sensitivity of −38.9 nm/(mg/mL) was obtained experimentally. The concentration DL for the MZI-based biosensor is calculated to be 2.57×10^{-4} mg/mL.

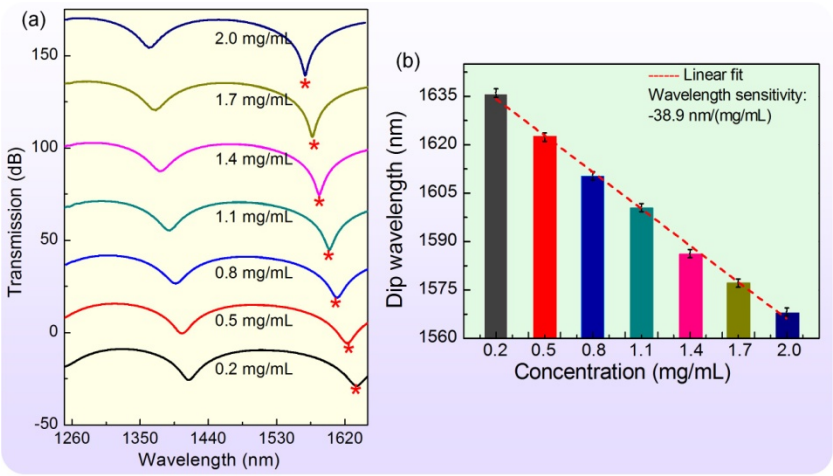

Fig. 5. (a) Transmission spectra evolution at different BSA concentrations. (b) Spectra shift dips at long wavelengths for different BSA concentration samples.

5. Conclusion

In summary, we have presented BSA concentration measurements acquired with a simple in-fiber MZI. The primary structure is a micro-cavity fabricated in the fiber core and cladding. Several micro-channels allow the biosensor to exchange information with surrounding media. A new fabrication technology involving chemical etching was utilized in this work. The minimum detectable RI variation (3.5×10^{-5} RIU), associated with an ultra-high RI sensitivity of −10,055 nm/RIU, allowed for differentiation of low BSA concentrations. A concentration sensitivity of −38.9 nm/(mg/mL) could be achieved with a low DL of 2.57×10^{-4} mg/mL. The MZI biosensor itself is simple, compact, and highly sensitive. As such, it is an excellent candidate for low-concentration BSA detection.

Funding

This work was supported by National Natural Science Foundation of China (grant nos. 61575128, 61425007 and 61635007), Guangdong Natural Science Foundation (grants nos. 2015A030313541, 2014B050504010 and 2014A030308007), Science and Technology Innovation Commission of Shenzhen (grants nos. JCYJ20160520163134575, JCYJ20160523113602609, JCYJ20150324141711611, JCYJ20150324141711614 and JCYJ20150324141711576), Personal Crew of Science and Technology Program of Shenzhen (GRCK2016082611242959) and Pearl River Scholar Fellowships